DOI: 10.26599/FSHW.2026.9251292

Contents lists available at SciOpen

Food Science and Human Wellness

journal homepage: https://www.sciopen.com/journal/2097-0765

China Food Publishing Co.

Maintenance of NO homeostasis by blue honeysuckle polyphenols *via* EGFR/PI3K/Akt signaling protects against high-altitude pulmonary edema

Guizhen Kan[a1], Huizhi Chen[a1], Weijie Wu[a], Xiangjun Fang[a], Hangjun Chen[a], Mohamed A. Farag[c], Ben Niu[a], Junwei Huo[b],Chaoyi Shen[a], Yan Xu[d*], Ruiling Liu[a*], Haiyan Gao[a*]

[a]*Key Laboratory of Post-Harvest Handling of Fruits, Ministry of Agriculture and Rural Affairs, Zhejiang Key Laboratory of Intelligent Food Logistic and Processing, Key laboratory of postharvest preservation and processing of fruits and vegetables, China National Light Industry, Food Science Institute, Zhejiang Academy of Agricultural Sciences, Hangzhou, 310021, China*

[b]*National-Local Joint Engineering Research Center for Development and Utilization of Small Fruits in Cold Regions, National Development and Reform Commission, College of Horticulture and Landscape Architecture, Northeast Agricultural University, Harbin, 150030, China*

[c]*Pharmacognosy Department, Faculty of Pharmacy, Cairo University, Kasr el Aini St., Cairo 11562, Egypt*

[d]*College of Food and Pharmaceutical Sciences, Zhejiang Ocean University, Zhoushan 316022, China*

ABSTRACT: High-altitude pulmonary edema (HAPE) is a serious high-altitude illness; Dexamethasone (DEX) is widely used, but its use is limited by adverse effects including gastrointestinal and metabolic disorders. Honeysuckle (*Lonicera caerulea* L.) is an emerging cold-region berry; its polyphenols (LCP) show anti-hypoxic, anti-fatigue, antioxidant, hepatoprotective, and nephroprotective effects. LCP enhanced hypoxic mouse pulmonary microvascular endothelial cells (PMVECs) viability by 36.55% ($P < 0.01$). In a hypobaric hypoxia-induced mouse HAPE model, LCP extended survival time by 4.38 min ($P < 0.01$) and improved pulmonary capillary integrity, shown by reduced alveolar exudation and lung water accumulation. LCP showed no apparent toxicity and oral bioavailability. Integrated mechanistic approaches (metabolomics, network pharmacology, molecular docking, ELISA, qRT-PCR, Western blotting) demonstrated significant downregulation of EGFR and Akt ($P < 0.01$). Collectively, LCP mitigates HAPE by suppressing oxidative stress and maintaining NO homeostasis *via* coordinated iNOS/eNOS regulation through the EGFR/PI3K/Akt pathway.

Keywords: *Lonicera caerulea* Polyphenols, High-Altitude Pulmonary Edema, EGFR/PI3K/Akt Pathway, NO Homeostasis

1. Introduction

Blue honeysuckle fruit, commonly known as honeyberry, is an emerging cold region berry that has attracted increasing attention in research on medicinal and edible plants. Its rich polyphenol content confers strong antioxidant properties[1]. *Lonicera caerulea* L. polyphenols (LCP) can effectively regulate several pro-inflammatory cytokines, supporting their pharmacological roles in hepatoprotection, nephroprotection, lipid-lowering, and diabetes prevention[2][3][4]. The representative monomeric compounds in LCP,

[1] These authors made equal contribution to this work.
***Corresponding author**
xuyan@zjou.edu.cn (Y. Xu), ruilingliu2005@163.com (R. Liu), spsghy@163.com (H. Gao)

Received 25 February 2026
Received in revised from 9 April 2026
Accepted 11 May 2026

Quercetin[5][6] and Luteolin[7], exhibit bioactive properties including protection against oxidative and mitochondrial damage, anti-cancer effects, and hypoxia tolerance. Notably, Luteolin inhibits the EGFR/PI3K/Akt and EGFR/ERK/AP-1 signaling pathways, thereby contributing to therapeutic effects against lung injury[8].

Growing interest in high-altitude tourism and mountaineering has increased exposure to hypobaric and hypoxic environments, leading to a higher incidence of altitude-related illnesses, particularly HAPE[9][10]. The prevalence of HAPE rises rapidly with increasing altitude, and its acute onset necessitates effective pharmacological strategies for its prevention and protection. DEX is currently a widely adopted first-line treatment, though its use is linked to gastrointestinal and metabolic complications[11][12]. Meanwhile, nifedipine, as a calcium channel blocker that dilates pulmonary arterioles is another remedy, although it can induce adverse effects including peripheral edema and hypotension[13].

Pulmonary microvascular endothelial cells (PMVECs) are crucial epithelial cells in HAPE. They constitute the primary cellular barrier of the pulmonary microcirculation and maintain the homeostasis of pulmonary vascular permeability. Hypoxia leads to excessive generation of intracellular reactive oxygen species (ROS), causing oxidative damage to DNA, lipids and other cellular components. This damage contributes to PMVECs dysfunction and apoptosis[14][15], thereby disrupting the pulmonary microenvironment, exacerbating vascular leakage and inflammation, and amplifying the symptoms of HAPE. Studies indicated that modulating oxidative stress levels can effectively alleviate the severity of HAPE[16][17]. Salidroside (SAL) has been demonstrated to alleviate hypoxia-induced decline in cell viability and reduce oxidative damage[18]. HAPE is associated with the elevated expression of multiple pro-inflammatory cytokines, including interferon gamma (IFN-γ), monocyte chemoattractant protein-1 (MCP-1), epidermal growth factor receptor (EGFR), interleukin-6 (IL-6), interleukin-1β (IL-1β), and tumor necrosis factor alpha (TNF-α)[19][20][21]. Phosphatidylinositol 3-kinase (PI3K), a downstream gene of EGFR, closely linked to the expression of protein kinase B (Akt) [8]. Following oxidative stress injury, Akt-mediated signaling regulates endothelial nitric oxide synthase (eNOS) to promote nitric oxide (NO) synthesis, which dilates pulmonary vessels, maintains vascular permeability, and stabilizes pulmonary blood pressure. Additionally, EGFR/PI3K/Akt pathway can modulate inducible nitric oxide synthase (iNOS) expression, excessive NO production and attenuating oxidative injury[22][23]. The human body mainly regulates NO and oxidative stress through the EGFR/PI3K/Akt pathway, with its activity correlating to the severity of HAPE symptoms.

In conclusion, discovering safe and effective interventions to prevent and treat HAPE is an urgent necessity. LCP represents a promising yet underexplored candidate, whose active monomeric constituents-such as luteolin and quercetin-exhibit significant bioactivity against HAPE. However, the synergistic effects of LCP components in HAPE intervention have not been systematically investigated. Therefore, this study focuses on elucidating the preventive and therapeutic effects of LCP on HAPE, exploring its underlying pathways, and validating its toxicity, bioavailability, and administration routes by assessing cell

viability and survival indices in experimental animals. These efforts aim to pave the way for subsequent human studies and offer a new perspective for the clinical management of high-altitude-related diseases.

2. Materials and methods

2.1 Material and reagents

Blue honeysuckle were procured from the College of Horticulture and Landscape Architecture at Northeast Agricultural University. Kits for detecting cell viability, apoptosis, and cell cycle were acquired from Beyotime Biotechnology Co., Ltd. (Shanghai, China). ELISA detection kits were acquired from Lun Changshuo Biotechnology Co., Ltd. (Xiamen, China). Reagents for RNA extraction, reverse transcription, and quantitative real-time PCR (qRT-PCR) were obtained from Vazyme Biotech Co., Ltd. (Nanjing, China). Materials required for Western blotting were purchased from Sevendelta Biotechnology Co., Ltd. (Beijing, China), and antibodies were sourced from GeneTex (Irving, Texas, USA). All remaining chemicals utilized in this study were either analytical or chromatography grade, obtained from Aladdin Biochemical Technology Co., Ltd. (Shanghai, China).

2.2 LCP purification

The extraction and purification of polyphenols from honeysuckle were performed following the protocol established by Chaovanalikit[24]. Briefly, fresh berries were washed, ground into powder under liquid nitrogen, and mixed with 65% ethanol at a solid-to-solvent ratio of 1:18 ($g \cdot mL^{-1}$). Extraction was performed on the sample mixture using ultrasound assistance, with the parameters set to 200 W and 45°C maintained over two hours. After extraction, the resulting solution was subjected to vacuum filtration twice for solid residue removal. The obtained filtrate was then concentrated to one-twentieth of its original volume by rotary evaporation. The concentrated extract was then purified using XAD-7 macroporous resin. The XAD-7 macroporous resin was pretreated by soaking in 95% ethanol for 24 h, washing with ultrapure water until odorless, then sequentially soaking in 5% HCl and 5% NaOH for 4 h each, and rinsing to neutrality with ultrapure water before use[25]. For static adsorption-desorption, the adsorption equilibrium time was 4 h and the desorption equilibrium time was 2 h. The sample loading concentration was 3.0 $mg \cdot mL^{-1}$ at pH 4. Desorption was performed with 95% ethanol (pH 7.0). In the dynamic adsorption-desorption experiment, the loading phase was conducted at a rate of 2 BV per hour, using a sample volume of 550 mL. For elution, the same flow rate of 2 BVh was applied. Prior to the step, the column was washed with 4 BV of water. The purified eluate was concentrated and lyophilized to obtain the purified polyphenol powder. The polyphenol yield after purification was calculated as follows:

$$\text{Polyphenol yield (\%)} = (\text{weight of purified LCP} / \text{weight of crude extract}) \times 100\%$$

2.3 Effect of LCP on cellular hypoxia tolerance

2.3.1 Cells

Pulmonary microvascular endothelial cells (PMVECs) were acquired from Procell Life Science & Technology Co., Ltd. located in Wuhan, China. Cells were routinely cultured under normoxic conditions at 37℃ in a humidified incubator containing 5% CO_2. To establish hypoxia, cells were cultured in a standard incubator (37℃, 5% CO_2) and a modular hypoxic chamber (37℃, 94% N_2, 5% CO_2, 1% O_2).

2.3.2 Cell viability assay

The cell viability assay was conducted based on an established protocol with minor adaptations[26]. Salidroside (SAL) alleviates hypoxia-induced reduction in cell viability and attenuates oxidative damage[18]. In brief, cells were prepared as a single suspension and plated in 96-well plates at a concentration of 5×10^4 cells per milliliter. After 24 h, cells were divided into the following groups based on preliminary experiments: normoxia control (NC), hypoxia (NH), hypoxia with LCP treatment (LCP-10, -15, -20, -25, -30, -35 $\mu g\cdot mL^{-1}$), and hypoxia with salidroside treatment (SAL-10, -15, -20, -25, -30, -35 $\mu g\cdot mL^{-1}$). Following 12 h of further incubation, the NC group remained in a standard incubator (Heracell VIOS 150i, Thermo Fisher, MA, USA), while the NH, LCP, and the group treated with SAL was placed into a modular hypoxia chamber (MIC-101, Billups-Rothenberg, CA, USA) and exposed to an atmosphere of 94% N_2, 5% CO_2, and 1% O_2 for 48 hours. After exposure to the specified conditions, the viability of the cells was evaluated by means of the Cell Counting Kit-8 (CCK-8), following the manufacturer's protocol precisely.

2.3.3 Cellular oxidative stress level

Based on the results from section 2.3.2, PMVECs were divided into four groups: NC, NH, LCP, and SAL. The optimal concentrations for LCP and SAL, determined by their anti-hypoxic efficacy, were selected for treatment. Cells were seeded into 6-well plates and cultured for 24 h. After administering the respective treatments, the NC group was maintained in a standard incubator, while the NH, LCP, and SAL groups were placed in a modular hypoxic chamber for 48 h. Intracellular ROS levels were then determined with the DCFH-DA fluorescent probe, following the supplier's instructions. Fluorescence was visualized and images were captured under non-fluorescent (NF), bright-field (BF), and dark-field (DF) modes on a Leica TCS SP8 DLS laser scanning confocal microscope (Hesse, Germany)[26].

2.3.4 Apoptosis and cell cycle

Cell apoptosis analysis was performed following the protocol established by Jiang[27]. Following the procedures outlined in section 2.3.3, PMVECs were harvested from all experimental groups and rinsed twice with phosphate-buffered saline (PBS). After adjusting the cell density to 1×10^6 cells per milliliter, apoptosis was evaluated with an Annexin V-FITC/PI detection kit, following the supplier's recommended procedures. Finally, sample analysis was performed on an Attune CytPix flow cytometer (Thermo Fisher, MA, USA), configured with an excitation wavelength of 488 nm and an emission wavelength of 530 nm.

For cell cycle analysis, the washed cell pellets were gently resuspended in 1 mL of 70% ethanol (chilled on ice) and then fixed at 4℃ overnight. According to the cell cycle detection kit manual, cells were stained

with propidium iodide (PI). The distribution of cells across different cell cycle phases was subsequently analyzed on the same flow cytometer, with the instrument parameters set to an excitation wavelength of 488 nm and an emission wavelength of 610 nm.

2.4 Animals

A total of 110 male BALB/c mice (18-22 g, specific pathogen-free grade) were purchased from Vital River Laboratory Animal Technology Co., Ltd. (Beijing, China; certificate number: 20250521Abzz06199990325). The mice were housed in the Animal Experiment Center of Zhejiang Academy of Agricultural Sciences under controlled conditions: temperature 25℃, a 12 h light and dark cycle, with free access to food and water. All experimental procedures were approved by the Animal Care and Ethics Committee of Zhejiang Academy of Agricultural Sciences (approval number: 25ZALA46). The sample size of each group was determined based on preliminary pre-experiments, relevant ethical guidelines for laboratory animals, and previously reported HAPE mouse models, which could guarantee sufficient statistical power for subsequent statistical analysis[29][30].

2.5 Effect of LCP on hypoxia tolerance in mice

Fifty male BALB/c mice were randomly divided into 10 groups (n = 5 per group) to conduct both normobaric hypoxia tolerance and acute hypobaric hypoxia experiments, with 5 groups randomly assigned to each test. The groups were as follows: blank control (BC, distilled water), low-dose LCP (LCP-L, 400 $mg \cdot kg^{-1}$), medium-dose LCP (LCP-M, 800 $mg \cdot kg^{-1}$), high-dose LCP (LCP-H, 1200 $mg \cdot kg^{-1}$), and Dexamethasone (Dex, 6 $mg \cdot kg^{-1}$). After a 2 weeks acclimatization period, all groups received oral gavage once daily for 3 weeks (volume: 20 $mL \cdot kg^{-1}$). For the Dex group, drug administration was performed only during the final 3 days, preceded by distilled water gavage. Normobaric hypoxia tolerance test: 60 min after the last administration, mice from the designated groups were individually placed into 200 mL airtight jars containing soda lime and filter paper. The time from sealing to respiratory arrest (cessation of abdominal movement) was recorded for each mouse. The mice from the remaining groups were transferred into a hypobaric chamber. The simulated altitude within the chamber was raised at 25 $m \cdot s^{-1}$ until reaching 10,000 m and held for 30 minutes. Survivors in each group were then counted. These experimental procedures were adapted from established protocols[28][29][30].

2.6 Effect of LCP on HAPE in Mice

2..6.1 Establishment of the mouse HAPE Model

Screening in the PMVECs hypoxia model showed that the optimal concentration of LCP was 25 $\mu g \cdot mL^{-1}$. Based on the body surface area (BSA) conversion principle and combined with the first-pass effect correction factor (1.6) for orally administered natural polyphenolic compounds, the equivalent oral dose for mice was calculated to be approximately 800 $mg \cdot kg^{-1}$. Acute toxicity preliminary experiments confirmed that LCP exhibited no obvious toxic reactions at a single oral dose of 2000 $mg \cdot kg^{-1}$. Therefore, the following

animal experiments were designed: A total of sixty mice were randomly assigned to six equal groups(n = 10 per group): normoxia control (NC, distilled water), high-altitude model (MOD, distilled water), low-dose LCP (LCP-L, 400 mg·kg^{-1}), medium-dose LCP (LCP-M, 800 mg·kg^{-1}), high-dose LCP (LCP-H, 1200 mg·kg^{-1}), and Dexamethasone (Dex, 6 mg·kg^{-1}). After completing the acclimatization and oral administration protocol, the HAPE model was induced. The NC group remained under standard local ambient conditions (altitude: 40 m; pressure: 101 kPa; oxygen partial pressure: 21 kPa; temperature: 25℃) for a period of three days. All remaining groups were transferred into a hypobaric hypoxia chamber (ProOx 811, TOW, ShangHai, China) and subjected to conditions simulating an altitude of 6500 m (chamber pressure: 42.0 kPa; oxygen partial pressure: 8.8 kPa; temperature: 25℃) for the same duration. The simulated altitude within the chamber was increased at a rate of 10 m·s^{-1}. Throughout the modeling period, gavage administration continued daily, along with routine replenishment of food and water. After modeling, mice received an intraperitoneal injection of 1% pentobarbital sodium for anesthesia. Blood samples were subsequently collected *via* orbital puncture, followed by euthanasia through cervical dislocation. The body surface was disinfected, and mice were then dissected. The lungs were excised, weighed, and processed for subsequent pathological analysis.

2.6.2 Body weight and food intake

Prior to the formal experiment, each mouse's body weight was measured and recorded. Subsequently, weights were measured and recorded at the same time each week and immediately before dissection. During the hypoxic exposure period, the hypobaric chamber was returned to normoxic conditions daily at 8:00 a.m. to replenish food and water. The remaining food was weighed each day, and the average daily food intake for each group over the three day modeling period was calculated.

2.6.3 Lung water content (LWC)

The lower left lung lobe was harvested and its wet weight was promptly determined with an electronic balance. Subsequently, the lobe was transferred to a glass dish and oven-dried at 60℃ until its weight stabilized. After allowing the sample to cool to ambient temperature, the final dry weight was recorded. The LWC was calculated as follows:

$$\text{LWC (\%)} = [(\text{wet weight} - \text{dry weight}) / \text{wet weight}] \times 100\%.$$

2.6.4 Organ index (OI)

Upon completion of blood collection, euthanasia was performed *via* cervical dislocation. The carcasses were then surface-disinfected and systematically dissected to isolate the lungs. Any superficial blood adhering to the harvested organs was carefully removed using filter paper before their wet weights were measured. The OI was subsequently determined by applying the following formula:

$$\text{OI (\%)} = (\text{organ weight} / \text{body weight}) \times 100\%.$$

2.6.5 Protein concentration in bronchoalveolar lavage fluid (BALF)

The lungs were carefully isolated and lavaged by slowly injecting and withdrawing 1.0 mL of sterile saline through the trachea for 3 repeated cycles, with a total lavage volume of 3 mL. The average recovery rate of BALF was approximately 85%. The pooled BALF was then centrifuged at 4℃ and 2500 rpm for 15 minutes[28]. After centrifugation, the supernatant was harvested, and its total protein content was quantified using a BCA protein assay kit, in strict adherence to the provided protocol. The protein concentration was normalized according to the actual recovered volume to ensure data accuracy. The BALF protein concentration was calculated as follows:

BALF protein concentration × (total lavage volume / actual recovered volume)

2.6.6 Histopathology

We carefully excised the right lower lobe of the lung, washed it with ice-cold saline to eliminate residual blood, and lightly blotted it dry with filter paper. The tissue samples were soaked in 4% paraformaldehyde and kept at 4℃ until full fixation and expansion were accomplished. The specimens were then dehydrated with a graded series of ethanol solutions, embedded in paraffin, and cut into 5 μm sections. For histological evaluation, these sections were stained with hematoxylin and eosin (H&E) and examined under an optical microscope. The remaining lung tissue was washed, immediately frozen in liquid nitrogen, and preserved at -80 ℃ for subsequent analysis.

2.6.7 Oxidative stress markers in lung tissue and serum

Frozen lung tissue samples were first pulverized into a fine powder within a liquid nitrogen chilled mortar. This powder was then homogenized on ice using cold PBS (1×, pH 7.4). The resulting homogenate was vigorously vortexed for 5 minutes at 4℃, followed by centrifugation at 1257 rad·s^{-1} for 15 minutes under the same temperature. After centrifugation, the clear supernatant was carefully collected for later biochemical tests. To assess antioxidant capacity, we measured the activity levels of superoxide dismutase (SOD), catalase (CAT), and glutathione (GSH) with commercially available test kits, strictly adhering to the accompanying protocols. For accurate comparison, all antioxidant activity data were normalized against the total protein concentration in each sample, which was determined separately using a BCA protein assay kit.

Orbital puncture blood samples were processed as follows: clotting at 37℃ (30 min), followed by centrifugation (15 min, 419 rad·s^{-1}, 4℃). The clarified yellowish serum was aliquoted in 100 μL volumes, labeled, and archived at -80℃ to avoid freeze-thaw damage. Quantification of serum nitric oxide (NO) and malondialdehyde (MDA) was carried out employing dedicated commercial kits, following the respective protocols.

2.6.8 Enzyme-linked immunosorbent assay (ELISA)

Contents of interferon-γ (IFN-γ), epidermal growth factor receptor (EGFR), and monocyte chemoattractant protein-1 (MCP-1) were quantified in the serum samples as detailed in section 2.6.1. Furthermore, levels of tumor necrosis factor-α (TNF-α), interleukin-6 (IL-6), and interleukin-1β (IL-1β) were

measured in the BALF obtained from section 2.6.5. All detections were conducted with corresponding ELISA kits, in strict accordance with the instructions provided by the manufacturers.

2.7 LCP identification

2.7.1 LC-Orbitrap HRMS analysis

The component of LCP was quantified *via* liquid chromatography coupled to Orbitrap high-resolution mass spectrometry (LC-Orbitrap HRMS). The analytical equipment comprised a Vanquish UPLC system (Thermo, USA) for chromatographic separation, connected to a Q Exactive HF X mass spectrometer (Thermo, USA) for detection. In terms of sample pretreatment, we precisely measured a 100 mg aliquot of the sample into a centrifuge tube, then introduced 0.1 mL of ice-cold water and vortex-mixed the mixture for 60 seconds. Subsequently, 0.4 mL of a pre-chilled methanol/acetonitrile solution (1:1, $v \cdot v^{-1}$) was introduced, followed by another 60-second vortex mixing step. Low-temperature ultrasonic extraction was performed for 30 min and repeated once. Pooled extracts were held at -20 ℃ for 1 hour to sediment proteins, then spun down at 1466 $rad \cdot s^{-1}$ for 20 min at 4 ℃. The supernatant was harvested and lyophilized, and the dried residue was redissolved in 200 μL of 30% acetonitrile, then subjected to vortexing and centrifugation (1466 $rad \cdot s^{-1}$, 15 min, 4℃). The obtained clarified supernatant was subsequently analyzed directly by LC-MS.

We derived the LC-MS parameters from a prior investigation conducted by Kusznierewicz[31]. In regard to LC separation, an ACQUITY UPLC HSS T3 column (Waters, USA) - featuring dimensions of 100 mm × 2.1 mm and a particle size of 1.8 μm - was employed. A binary mobile phase setup was adopted for chromatographic separation: phase A was composed of 0.1% formic acid dissolved in water, while phase B consisted of acetonitrile. Gradient elution was carried out at a steady flow rate of 0.3 $mL \cdot min^{-1}$, with the column temperature kept constant at 40℃, and the injection volume was fixed at 5 μL. The detailed gradient program was implemented as follows: 0-1 min, 100% phase A; 1-12 min, a linear reduction from 100% to 5% phase A; 12-13 min, maintenance at 5% phase A; 13-13.1 min, a rapid revert to 100% phase A; and 13.1-17 min, re-equilibration with 100% phase A.

Mass spectrometric detection was conducted using an LC-Orbitrap HRMS platform fitted with an electrospray ionization (ESI) source. The ESI source operated at: sheath gas flow 40 arbitrary units, auxiliary gas flow 10 arbitrary units, spray voltage +3000 V (positive mode)/-2800 V (negative mode), ion transfer tube temperature 320℃, and vaporizer temperature 350℃. Data acquisition adopted Full-MS/dd-MS^2 mode with rapid polarity switching between positive and negative modes. Full-scan spectra covered m/z 70-1050 at 70,000 resolutions, while 17,500 resolution and 30 eV normalized collision energy were applied for tandem mass spectrometry (MS^2)[32].

Quality control (QC) samples were prepared by mixing equal volumes of all experimental sample supernatants to monitor LC-Orbitrap HRMS reliability. During the analysis, one QC sample was injected every 3 experimental samples to evaluate instrument precision and reproducibility. For stability assessment,

RSD of retention time and peak area of typical polyphenols was calculated, with all RSD < 5% ensuring good stability and reliable data.

2.7.2 Characteristic peak identification

We processed the raw data utilizing Progenesis QI software (version 2.4). Characteristic peaks were extracted from the total ion chromatogram (TIC) using the following criterion: the retention time (RT) shift should not exceed ± 0.1 min, a mass accuracy ≤ 5 ppm (matching Orbitrap HRMS precision), and a peak intensity threshold of 1×10^4. RT drift was aligned across all samples, and missing values in peaks were imputed. Peak reproducibility was verified using pooled quality control (QC) samples ($n = 6$), with the acceptance criterion set at a relative standard deviation (RSD) of ≤ 30%. Peaks originating from matrix interference were excluded by comparison with blank solvent (ultrapure water) controls, resulting in a final set of qualified characteristic peaks.

Metabolite identification was performed *via* a three step process: primary mass spectrometry matching, secondary mass spectrometry confirmation, and hierarchical annotation. First, qualified peaks were matched against the HMDB v5.2, METLIN v2024, FoodDB v2.1, and KEGG v107 databases based on accurate m/z and retention time (RT) values, with analyses performed independently in both positive and negative ionization polarities. Subsequently, the MS^2 fragment spectra of characteristic peaks, obtained through data-dependent acquisition (DDA), were compared against database reference spectra. A similarity threshold of ≥70% was applied to discriminate isomers. For key metabolites such as cyanidin-3-glucoside, Level 1 identification was achieved by analyzing authentic standards under identical LC-MS conditions and confirming consistency in m/z, RT, and MS^2 fragmentation patterns. Annotation levels were assigned according to established standards: Level 1 (validated with standards), Level 2 (matched by MS^2), and Level 3 (matched only by MS^1).

2.8 Network pharmacology and molecular docking

2.8.1 Screening of pharmacodynamic components

The major components of honeysuckle identified by LC-Orbitrap HRMS were entered into TCMSP (Traditional Chinese Medicine Systems Pharmacology Database and Analysis Platform, https://old.tcmsp-e.com/tcmsp.php) and Herb database (http://herb.ac.cn/), then screened by oral bioavailability (OB) ≥ 20% and drug-likeness (DL) ≥ 0.1.

2.8.2 Screening of components and disease-related targets

Potential protein targets of the identified active compounds were retrieved from several online pharmacological resources, namely the TCMSP, the Traditional Chinese Medicine Integrated Database (TCMID; http://www.megabionet.org/tcmid/), and the STITCH database (http://stitch.embl.de/). Separately, disease-related targets for HAPE were retrieved by querying the term in the DisGeNET (http://www.disgenet.org/), GeneCards (https://www.genecards.org/) databases with the species filter set to

Homo sapiens. Prior to analysis, duplicate entries were cleared from the compound-target and disease-target gene lists. The resulting unique target lists were then submitted to the jvenn online platform to generate a Venn diagram identifying the overlapping targets.

2.8.3 Construction of Component-Disease-Target Network

The candidate target names identified through screening were first converted into official gene symbols. These standardized symbols were subsequently uploaded to the STRING database (https://string-db.org/) for the construction of a protein-protein interaction (PPI) network. Data derived from the component-target, disease-target and the newly generated PPI networks were integrated. The integrated network was finally assembled and graphically represented using Cytoscape software (version 3.11).

2.8.4 Gene ontology (GO) and kyoto encyclopedia of genes and genomes (KEGG) enrichment analysis

Core target genes underwent functional enrichment analysis *via* the DAVID database (https://david.ncifcrf.gov/). GO and KEGG pathway analyses were conducted in *Homo sapiens* with a significance threshold of $P < 0.05$.

2.8.5 Acquisition and preparation of receptors and ligands

The structures of the proteins of interest were acquired by querying both the UniProt and PDB databases. Using PyMOL software, the receptor files underwent preparation through removing water molecules and adding hydrogen atoms. The ligands were drawn in ChemDraw, saved in SDF format, and subsequently converted to MOL2 format. All structures were then processed with AutoDockTools (version 1.5.7) to remove water, add polar hydrogens, assign charges, and define rotatable bonds for the ligands.

2.8.6 Docking box setup and molecular docking

Using AutoDockTools 1.5.7, the grid box center was defined based on the active site coordinates, and its dimensions were adjusted to fully encompass the binding pocket. A config.txt file was generated to record all relevant docking parameters. Enter the command in AutoDock Vina: vina --config config.txt. The active components previously screened in Section 2.8.1 were subjected to final selection based on two criteria: a ligand-receptor binding energy < -4.5 kcal·mol^{-1}, and the formation of hydrogen bonds or hydrophobic interactions with key amino acid residues at the active sites.

2.9 Investigation into the molecular mechanisms of LCP in the prevention and treatment of HAPE

2.9.1 Quantitative real-time polymerase chain reaction (Egfr、Pi3k、Akt、Nos2)

Left lower lung tissue was ground into fine powder under liquid nitrogen. Total RNA was extracted with a kit and stored at -80℃. Reverse transcription was performed *via* thermal cycler: cDNA synthesis at 42℃ for 60 min, followed by enzyme inactivation at 70℃ for 10 min. Quantified cDNA was stored at -20℃. For qPCR (7500 Real-Time PCR System, Thermo Fisher), key parameters: initial denaturation at 95℃ for 3 min; forty

cycles of 95℃ for 10 s (denaturation) and 60℃ for 30 s (annealing/extension, fluorescence acquisition); melt curve (95℃ 15 s, 60℃ 1 min, 95℃ 15 s). All target genes were analyzed in triplicate ($n = 3$).

2.9.2 Western blot

Lung tissues were homogenized and lysed in RIPA buffer (1% PMSF). Protein concentrations were determined and normalized. Proteins were separated by 10% SDS-PAGE: stacking gel at 80 V for 30 min, separating gel at 120 V for 1 h. Subsequently, proteins were transferred onto a PVDF membrane, which was blocked with 5% skim milk for 2 h at room temperature, followed by overnight incubation at 4℃ with gentle shaking in specific primary antibodies (all diluted 1:500) against the following targets: EGFR, phospho epidermal growth factor receptor (Tyr1068) (p-EGFR), phosphatidylinositol 3-kinase p85 (PI3K p85), phospho-phosphatidylinositol 3-kinase p85 (Tyr458) (p-PI3K p85), protein kinase B (Akt), phospho-Akt (Ser473) (p-Akt), nitric oxide synthase 2, inducible (iNOS), and nitric oxide synthase 3, endothelial (eNOS). Post-primary antibody incubation, the membrane was washed 6× with 1× TBST (8 min), then incubated for 2 h at room temperature with gentle shaking using HRP-conjugated secondary antibodies (anti-mouse/anti-rabbit, diluted 1:5000). The washing step was repeated as above. Finally, the membrane was developed, and band intensities were quantified using β-actin as the loading control.

2.10 Statistical analysis

Data are presented as mean ± standard error of the mean (SEM). Statistical analysis was performed using GraphPad Prism version 8.0.2. One-way analysis of variance (ANOVA) followed by Tukey's post hoc test was used to determine significant differences, with ($P < 0.05$) considered statistically significant.

3. Results

3.1 LCP enhances hypoxia tolerance in PMVECs and protects normal cell growth and proliferation

To evaluate the hypoxia tolerance of LCP, the purity of the extracted and purified LCP was determined to be up to 89.56%, demonstrating stable purification efficacy. six different concentrations of LCP and the positive control drug SAL were used to treat the cells. Their effects on PMVECs viability under hypoxic conditions were assessed to determine whether LCP possesses anti hypoxic efficacy. Hypoxia markedly decreased the relative viability of PMVECs ($P < 0.01$), as presented in Figs. 1A and 1B. The cellular hypoxia tolerance improved in response to increasing concentrations of both LCP and SAL, peaking at 25 $\mu g \cdot mL^{-1}$ for LCP and 15 $\mu g \cdot mL^{-1}$ for SAL. Compared with the NH group, these treatments increased viability by 36.55% and 35.02%, respectively.

To determine whether LCP could alleviate hypoxic oxidative injury, intracellular ROS levels were measured as a representative marker. Confocal microscopy imaging (Fig. 1C) revealed the strongest fluorescence signal in the NH group. As quantified by relative fluorescence intensity (Fig. 1D), ROS in the NH group was 2.63 -fold that of the NC group, 1.68 -fold that of the LCP-25 group ($P < 0.01$). These results

demonstrate that LCP treatment significantly reduced intracellular ROS accumulation in PMVECs, thereby alleviating oxidative stress injury.

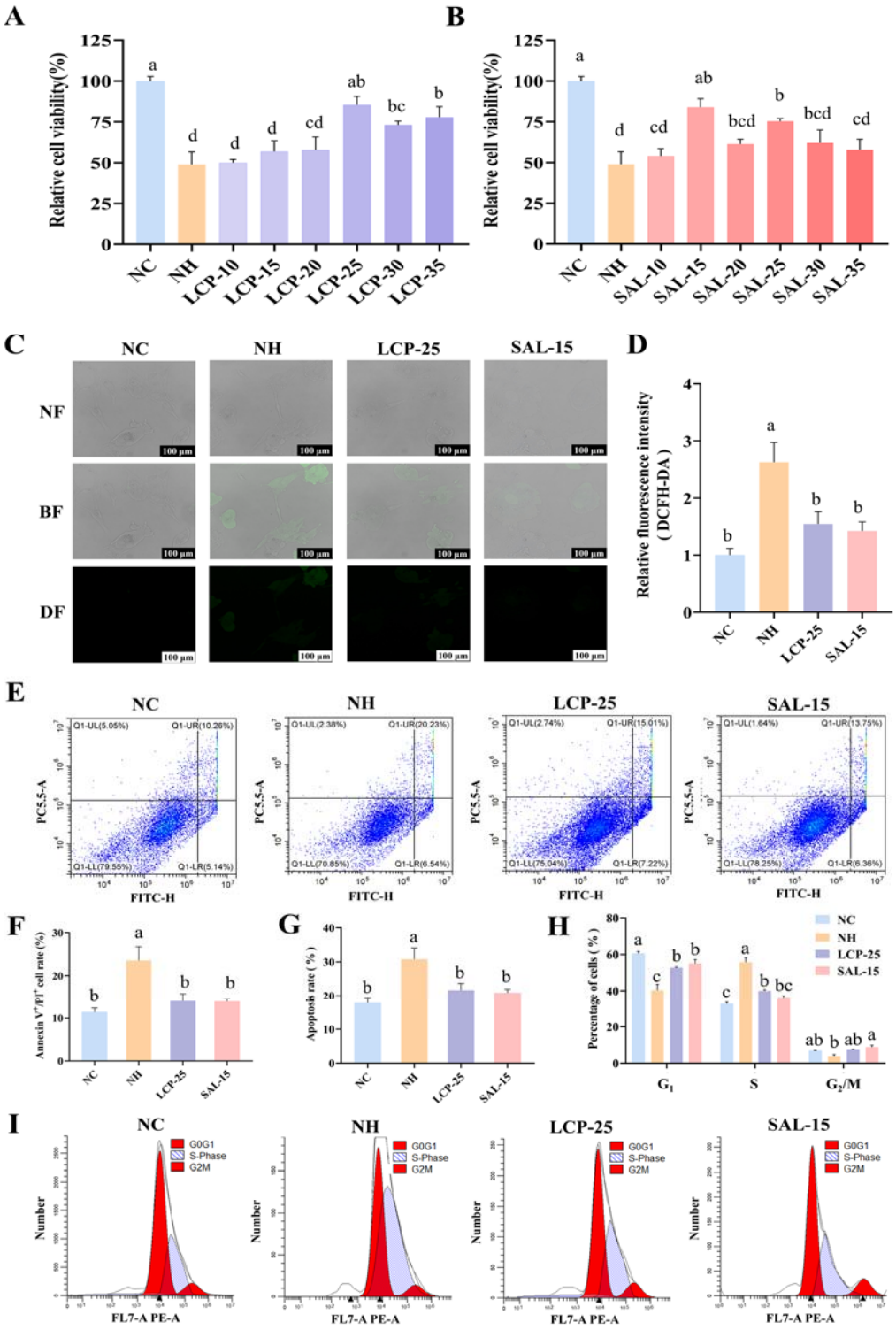


Fig. 1. Effect of LCP on hypoxic pulmonary microvascular endothelial cells (PMVECs). (A) Relative viability of PMVECs treated with different concentrations of LCP. (B) Relative viability of PMVECs treated with different concentrations of salidroside (SAL). (C) Representative fluorescence images showing intracellular ROS levels in different treatment groups. (D) Quantitative analysis of relative ROS fluorescence intensity (DCFH-DA) in PMVECs. (E) Apoptosis analysis of PMVECs under different treatments. (F) Proportion of Annexin V^+/PI^+ cells in different treatment groups. (G) Apoptotic rate of PMVECs in different groups. (H) Cell cycle distribution of PMVECs in different groups. (I) Representative cell cycle profiles of PMVECs. Experiments were performed in triplicate ($n = 3$). Different lowercase letters indicate statistically significant differences among groups ($P < 0.05$), while the same letter indicates no significant difference.

Alleviating apoptosis provides a more direct reflection of a compound's anti-hypoxic capacity. Post-hypoxia, a significant 9.97% elevation in PMVEC apoptosis was detected in the NH group versus the NC group (Figs. 1E-G; $P < 0.01$). In contrast, neither the LCP-25 nor the SAL-15 group exhibited any significant difference relative to the NC group ($P > 0.05$). The Annexin V^+/PI^+ cell ratio showed a strong correlation with the overall apoptotic proportion. These results indicate that hypoxia drives cells rapidly into late apoptosis or necrosis, while LCP and SAL effectively attenuate this apoptotic response.

3.2 LCP helps maintain normal proliferative behavior under hypoxia.

Flow cytometry analysis (Figs. 1H and 1I) indicated that hypoxia promoted the G_1-to-S transition but did not significantly alter the G_2/M phase cell population ($P > 0.05$), resulting in S-phase arrest in PMVECs. Treatment with LCP or SAL activated the S/G_2 checkpoint, allowing cells to resume normal cycling. This suggests that both compounds alleviate hypoxia-induced S-phase arrest in PMVECs.

3.3 LCP improves hypoxia tolerance in mice

As indicated in Table. 1, pretreatment with LCP enhanced survival duration and increased survival numbers across all dose groups relative to the BC group. In the normobaric hypoxia model, the survival time was extended by 3.65 min in the LCP-L group ($P < 0.05$). Furthermore, the LCP-M, LCP-H, and Dex groups demonstrated markedly longer survival times ($P < 0.01$).

Table. 1. LCP resistance to atmospheric hypoxia results in mice ($n = 5$).

Groups	Dose/ ($mg \cdot kg^{-1}$)	Survival time(min)	Elongation rate(%)
BC	0	27.05±1.82	——
LCP-L	400	30.70±2.52*	13.52%
LCP-M	800	34.46±2.01**	27.40%
LCP-H	1200	35.08±2.15**	29.71%
DEX	6	35.25±1.94**	30.31%

Compared with BC group: $P * < 0.05$; $P ** < 0.01$.

As shown in Table. 2, the survival rate in the LCP-L group was increased by 30%. In the LCP-M and LCP-H groups, the survival rate increased by 55% in both groups.

Table. 2. LCP resistance to anti-acute hypoxia results in mice ($n = 5$).

Groups	Dose/($mg \cdot kg^{1}$)	Survival number	Survival rate(%)
BC	0	2	20%
LCP-L	400	4^{*}	50%
LCP-M	800	6^{**}	75%
LCP-H	1200	6^{**}	75%
DEX	6	5^{**}	62.5%

Compared with BC group: $P *< 0.05$; $P **< 0.01$.

3.4 LCP ameliorates body weight, food intake, pulmonary function, and histomorphology in mice with HAPE.

An overview of the critical in vivo experimental workflow in mice is provided in Fig. 2A.Changes in body weight and food intake (Figs. 2B-D) under simulated high altitude conditions provided a direct assessment of overall health status and disease severity. Mice in the LCP treated groups showed increased body weight gain compared with the MOD group. During the modeling period, the LCP-M group demonstrated increased food consumption ($P < 0.05$). Conversely, mice in the MOD group showed a marked reduction in average body weight relative to the NC group ($P < 0.01$). Taken together with the reduced food consumption, these data indicate that mice in the MOD group were in a physiologically compromised state during hypoxic exposure.

LCP reduced LWC (Fig. 2E) and the lung OI (Fig. 2F) in mice, directly reflecting decreased pulmonary edema. All treatment groups exhibited lower lung water content relative to the MOD group. Specifically, the LCP-M group demonstrated a 3.54% reduction compared with the MOD group. The decreases in the LCP-H and DEX groups were more pronounced, amounting to 5.18% and 5.43%, respectively ($P < 0.01$). The lung OI in the normoxic NC group remained within the normal range, whereas the MOD group showed an increase of 4.80 $g \cdot kg^{-1}$ compared with the NC group. LCP-H treatment significantly lowered the OI by 4.01 $g \cdot kg^{-1}$ ($P < 0.01$). The influence of LCP on lung water content and OI exhibited a dose-response relationship, where the LCP-H group displayed the most pronounced improvements. The correlation between these two parameters mutually supported the conclusion, confirming LCP's efficacy in alleviating HAPE-related pulmonary edema.

Elevated protein concentration in BALF (Fig. 2G) indicates pulmonary vascular injury and increased permeability, a phenomenon ameliorated by LCP treatment. The level of protein in the BALF was markedly elevated in the MOD group compared to the NC group. All manipulation groups showed reduced BALF protein content compared with the MOD group, with significant decreases in the LCP-L ($P < 0.05$), in LCP-M, LCP-H, DEX groups $P < 0.01$. The observation that the lung OI was significantly lowered only in the LCP-H group ($P < 0.01$), while LCP-L and LCP-M groups still exhibited high LWC, suggests that the apparent reduction in protein concentration in the latter groups may be partly due to dilution by residual edema fluid.

Histopathological examination (Fig. 2H) revealed clear lung architecture, normal alveolar wall thickness, uniform alveolar spaces, with lung tissues from the NC group remaining clear of inflammatory cells. Tissues from the MOD group, however, revealed extensive infiltration of such cells within the interstitial. alveolar septa, and alveolar spaces (indicated by arrows), along with serous exudate filling the alveoli, capillary dilation, congestion, and increased vascular permeability. LCP treatment at different concentrations reduced alveolar inflammatory cells to varying degrees. Notably, the LCP-H and DEX groups decreased alveolar exudate and presented more uniform, well-preserved lung tissue structure compared with the LCP-L and LCP-M groups. Taken together, these results demonstrate that the LCP-H group produced the most pronounced amelioration of HAPE-associated pathology.

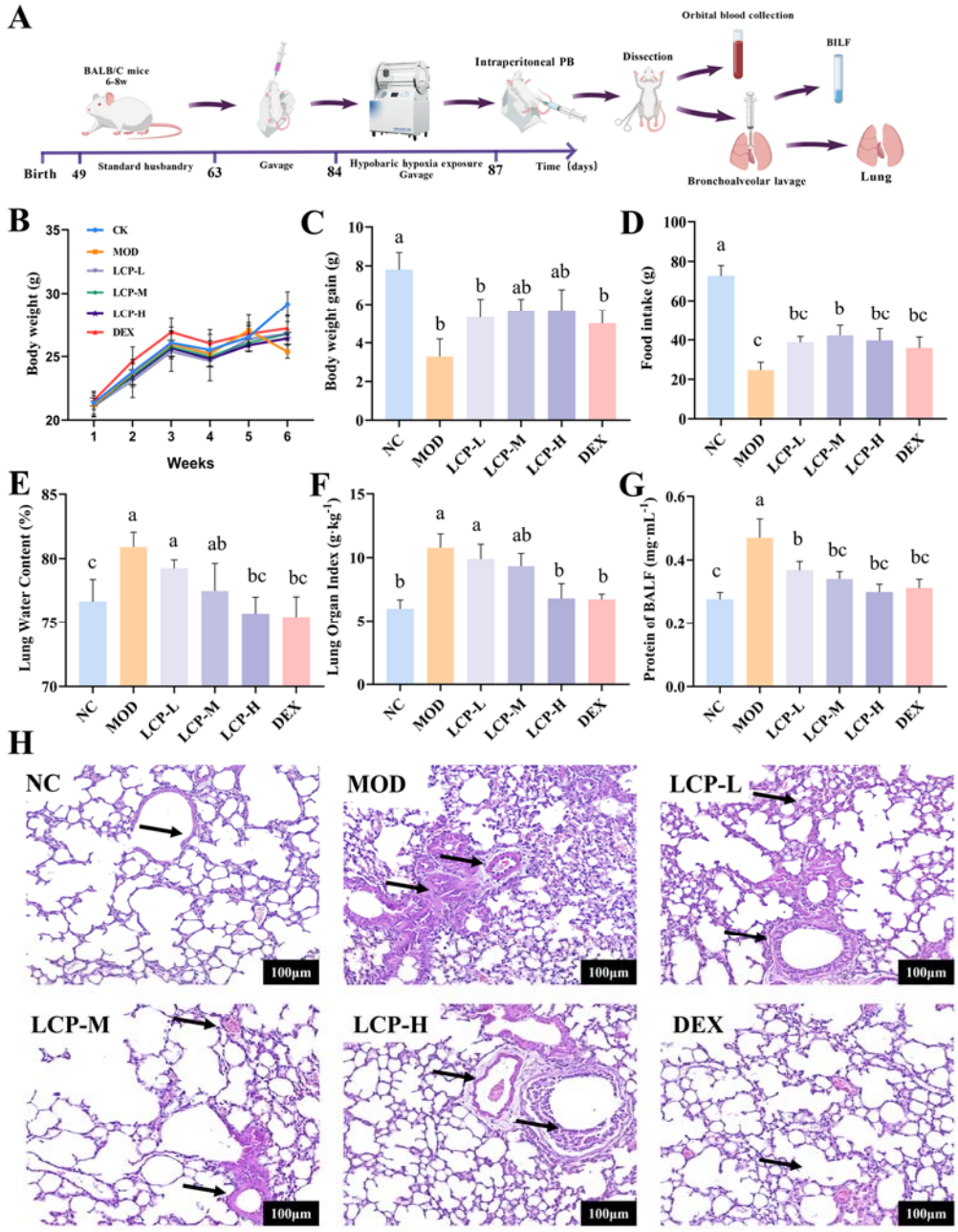


Fig. 2. Schematic of the animal experiment and analysis of pulmonary basic indices and histopathology. (A) Flowchart of the experimental procedure and treatment groups in mice. (B) Body weight change trends over time. (C) Net body weight gain. (D) Total food intake during the modeling period for each group. (E) Lung water content (LWC) (F). Lung organ index (G). Total protein concentration in bronchoalveolar lavage fluid (BALF). (H) Histopathological images of the right lower lung tissue. The right lower lung tissue was collected from three randomly selected mice per group, with each tissue section analyzed in triplicate ($n = 3$). Different lowercase letters indicate statistically significant differences among groups ($P < 0.05$), while the same letter indicates no significant difference.

3.5 LCP ameliorates oxidative stress and suppresses inflammatory cytokine release in mice

As shown in Fig. 3A, measuring oxidative stress levels serves as an important approach for assessing HAPE severity. Assays of lung tissue reflect local oxidative stress, while serum measurements indicate systemic oxidative damage. CAT, GSH, and SOD activities measured in lung tissue were all significantly reduced in the MOD group compared to the NC group ($P < 0.01$). LCP treatment ameliorated these indicators to varying degrees. CAT activity in the LCP-M group increased by 16.16 U·mg prot^{-1} relative to the

MOD group, an improvement superior to that of the DEX group (14.73 U·mg prot^{-1}). GSH content was elevated by 2.58, 2.74 μg·mg prot^{-1} in the LCP-H, DEX groups, respectively. The restoration of SOD activity in lung tissues by LCP followed a dose-responsive pattern, particularly in the LCP-M and LCP-H groups, where improvements were highly significant ($P < 0.01$). Serum levels of MDA and NO (Fig 3A) were also improved. All LCP-treated groups reduced MDA levels ($P < 0.01$) and performed better than the DEX group. After LCP treatment, NO levels decreased by 40.80% in the LCP-H group ($P < 0.01$). These results align with the ROS findings in section 3.1, confirming that LCP mitigates oxidative damage across experimental models.

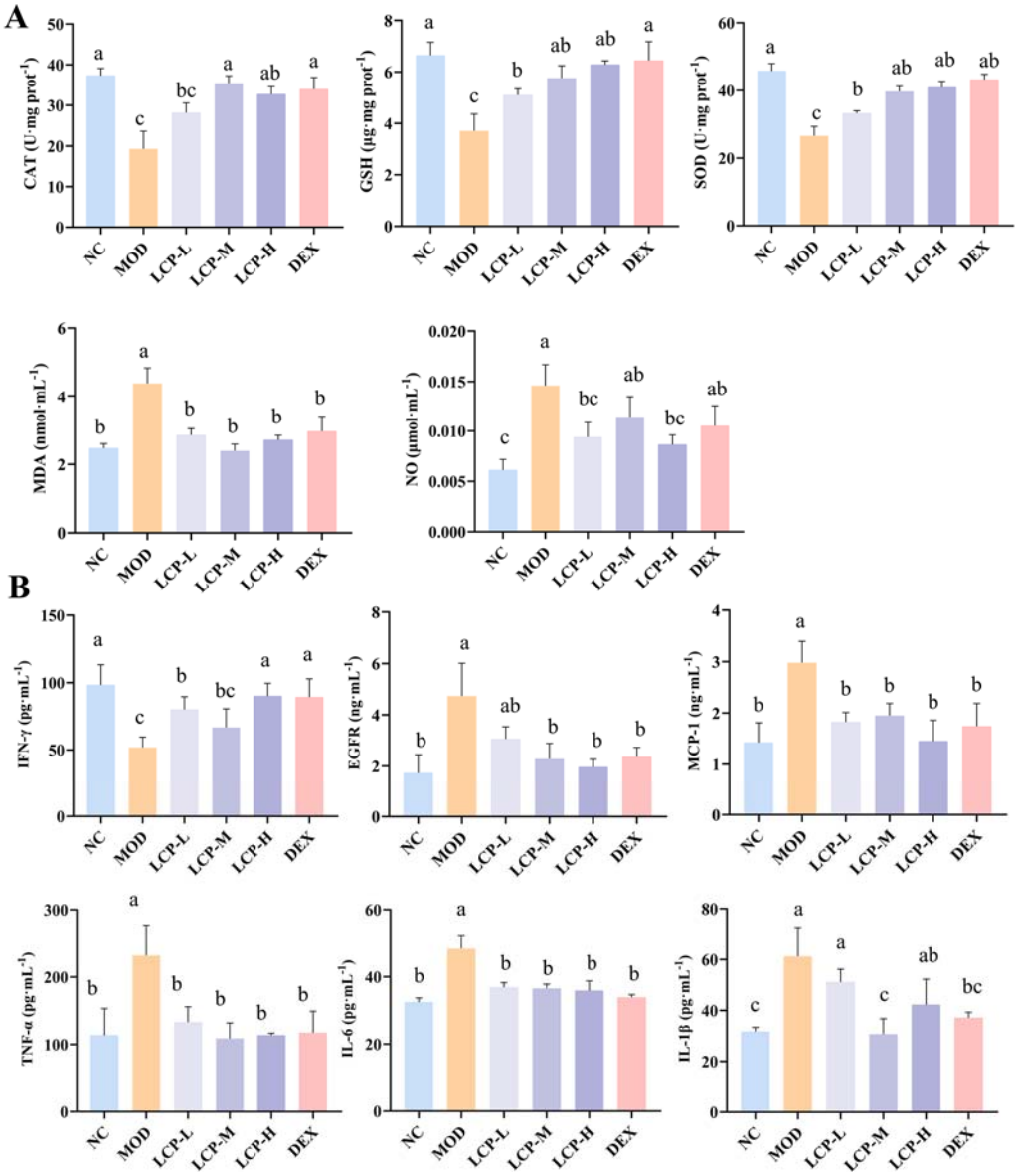


Fig. 3. Measurement of oxidative stress and inflammatory cytokine levels in mice. (A) Determination of CAT, GSH, and SOD activities in lung tissues, as well as MDA and NO levels in serum. (B) Assessment of IFN-γ, EGFR, and MCP-1 levels in serum, and TNF-α, IL-6, and IL-1β levels in bronchoalveolar lavage fluid (BALF). Experiments were performed in triplicate (n = 3). Different lowercase letters indicate statistically significant differences among groups ($P < 0.05$), while the same letter indicates no significant difference.

HAPE promotes the release of inflammatory cytokines (Fig. 3B). The levels of these cytokines directly reflect the onset, progression, and severity of HAPE. Pretreatment with LCP or DEX led to varying degrees of recovery in serum IFN-γ levels. Compared with the MOD group, the LCP-H group showed an increase of

38.12 pg·mL^{-1}. Elevated EGFR expression enhances the production of the pro-inflammatory chemokine MCP-1, thereby exacerbating inflammation. LCP at all concentrations treatment reduced EGFR expression in a dose dependent manner. No statistically significant difference was observed between the LCP-H, NC groups ($P > 0.05$). Contrast, the LCP-H group differed markedly from the MOD group ($P < 0.01$). Furthermore, its regulatory effect on MCP-1 levels surpassed that achieved by the DEX group.Furthermore, pretreatment with LCP effectively reduced TNF-α, IL-6, and IL-1β level. The LCP-M group showed a strong regulatory effect on TNF-α, IL-1β, decreasing their concentrations by 122.96 and 10.12 pg·mL^{-1}, respectively, compared with the MOD ($P < 0.01$). Notably, LCP exhibited a significant suppressive effect on IL-6 even at low concentrations.

3.6 Metabolites profiling of LCP secondary metabolites

To identify the active constituents in LCP, the extract was analyzed by LC-Orbitrap HRMS. Through identification and screening, 63 characteristic peaks were detected, among which 60 were qualified (Fig. 4A). The remaining 3 peaks were excluded due to low signal-to-noise ratio, poor spectral matching, and lack of valid fragment ions, failing to meet qualitative identification criteria. These included 32 phenolic compounds, 20 flavonoids, and 12 phenolic acids and other phenolic derivatives.

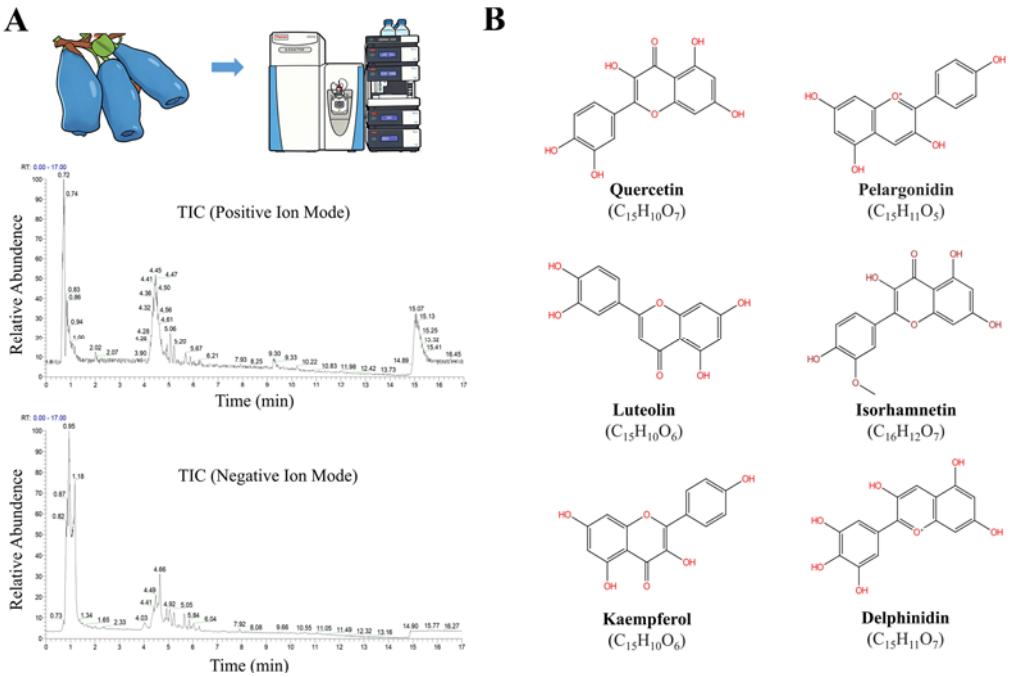


Fig. 4. Identification of purified polyphenols from *Lonicera caerulea* L. (LCP) (A) Representative total ion chromatograms (TIC) of LCP obtained by UHPLC-Q Exactive analysis in positive and negative ion modes. ($n = 3$). (B) Two-dimensional chemical structures of the key bioactive compounds identified after final screening of LCP.

3.7 Ligand-receptor molecular docking visualization and feasibility analysis

This section predicted the active components and molecular mechanisms of honeysuckle against HAPE by multiple methods. The compounds characterized in Section 3.5 underwent screening according to the method detailed in Section 2.8.1. Following this process, eight compounds (Quercetin, Pelargonidin, Luteolin, Isorhamnetin, Kaempferol, Delphinidin, Catechin, and Cyanidin) were identified as meeting the

specified criteria and were therefore selected as candidate compounds. Using Cytoscape 3.11, we mapped the interaction network between honeysuckle's active components and HAPE-related targets. This analysis identified 58 common targets shared by honeysuckle and HAPE (Fig. 5A). Core targets, including Akt, Peroxisome Proliferator-Activated Receptor Gamma (PPARG), IL-6, and EGFR, demonstrated robust interactions within the network (Figs. 5B-D). Functional enrichment analysis based on Gene Ontology (GO) further identified multiple biological processes that were significantly enriched. Including steroid binding, estrogen response element binding, and positive regulation of nitric oxide biosynthetic process (Fig. 5E). Subsequent KEGG pathway analysis revealed that nitrogen metabolism and pathways in cancer were prominently enriched (Fig. 5F).

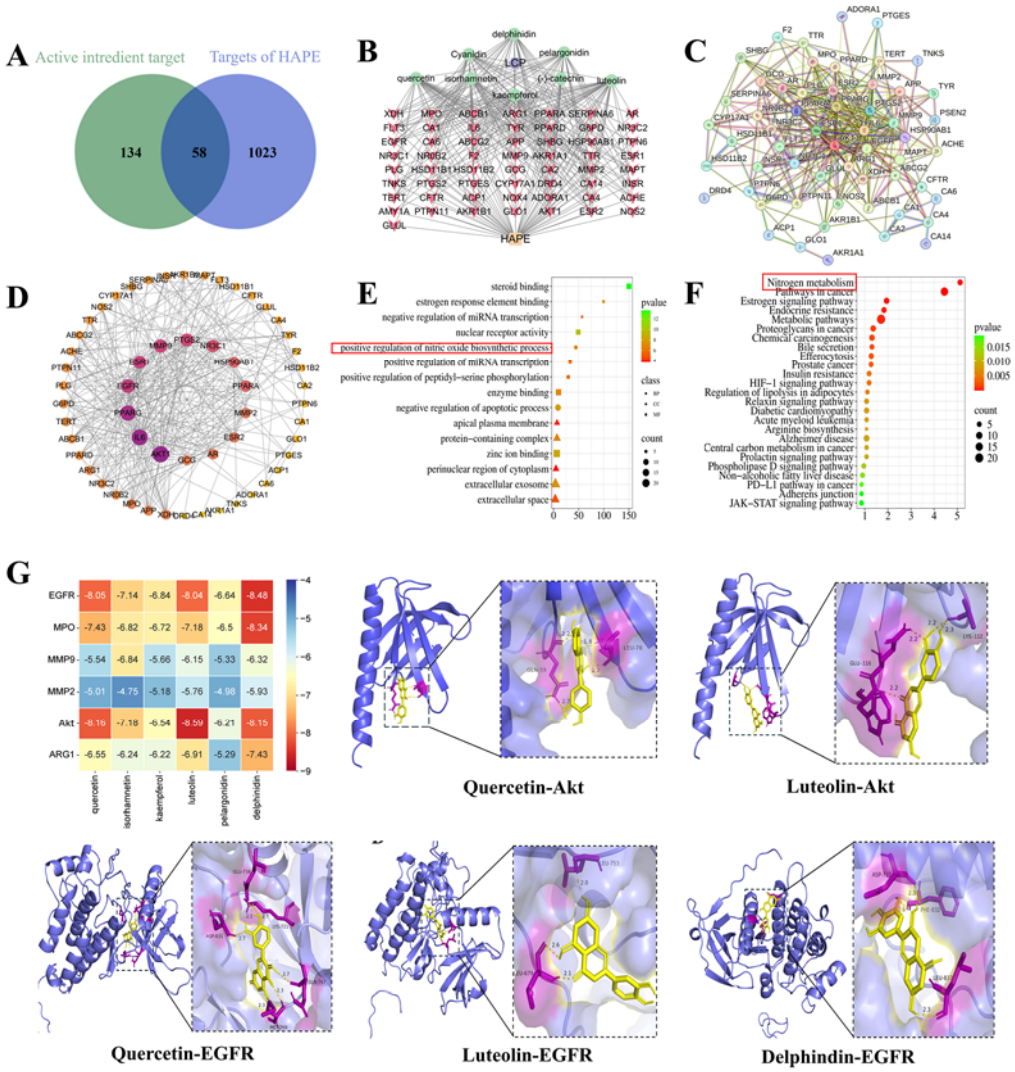


Fig. 5. Network pharmacology and molecular docking analysis of LCP in relation to High-altitude pulmonary edema (HAPE) targets. (A) Venn diagram showing the overlapping targets between active components of honeysuckle and HAPE-related genes. (B) "honeysuckle-Active Components-HAPE-Targets" interaction network. (C, D) Protein-protein interaction (PPI) networks of the shared targets. (E) Gene Ontology (GO) enrichment analysis of biological processes. (F) Kyoto Encyclopedia of Genes and Genomes (KEGG) pathway enrichment analysis. (G) Heatmap of ligand-receptor binding energies (≤ -4.5 kcal·mol^{-1}). Molecular docking visualization and binding energy analysis of Quercetin with Akt, Luteolin with Akt, Quercetin with EGFR, Luteolin with EGFR, and Delphinidin with EGFR.

This validation involved assessing hydrogen bonding energies and binding energies. Based on the binding energy analysis (ligand-receptor binding energy ≤ -4.5 kcal·mol^{-1}), 6 ligands (Quercetin,

Pelargonidin, Luteolin, Isorhamnetin, Kaempferol, and Delphinidin) demonstrated favorable binding capabilities with the receptors(Fig. 4B, Table. 3). Luteolin (Flavone) binds to Akt with a binding energy of -8.59 kcal·mol^{-1}, exhibiting the strongest binding affinity. The Akt and EGFR exhibited strong binding characteristics specifically with Quercetin, Luteolin, and Delphinidin (Fig. 5G).

Table. 3. Oral bioavailability (OB) and drug-likeness (DL) of the finally screened polyphenolic compounds from LCP.

No.	Molecule ID	Molecule name	Molecular formula	OB (%)	DL
1	MOL000098	Quercetin	$C_{15}H_{10}O_7$	46.43	0.28
2	MOL001004	Pelargonidin	$C_{15}H_{11}O_5^+$	37.99	0.21
3	MOL000006	Luteolin	$C_{15}H_{10}O_6$	36.16	0.25
4	MOL000354	Isorhamnetin	$C_{16}H_{12}O_7$	49.60	0.31
5	MOL000422	Kaempferol	$C_{15}H_{10}O_6$	41.88	0.24
6	MOL004798	Delphinidin	$C_{15}H_{11}O_7^+$	40.63	0.28

3.8 LCP alleviates HAPE symptoms by regulating iNOS/eNOS to control NO production

LCP alleviates HAPE symptoms through potential molecular mechanisms, and the present study verified the strong correlation between the corresponding genes predicted in Section 3.7 and HAPE. Both LCP-M and DEX treatments markedly suppressed *Egfr* expression ($P < 0.01$). The LCP-M and LCP-H groups effectively and consistently downregulated the expression of *Pi3k*, *Akt*, and *Nos2*, demonstrating significant inhibition relative to the MOD group (Fig. 6A ; $P < 0.01$).

Western blot analysis (Figs. 6B and 6C) revealed that the relative protein expression levels of p-EGFR and iNOS were markedly elevated in the MOD group relative to the NC group. Specifically, p-EGFR expression increased by 2.64-fold, while iNOS expression rose by 4.62-fold. This marked upregulation suggests a trend of severe oxidative stress injury, which aligns with the qRT-PCR findings presented in Fig. 6A. Although total PI3K and Akt immunofluorescence did not differ significantly among groups ($P > 0.05$), markedly higher signals for phosphorylated p-PI3K and p-Akt were detected in the MOD group. This may be attributed to enhanced expression of the upstream gene *Egfr* (Fig. 6A), which promotes the synthesis of PI3K and Akt proteins, thereby achieving a dynamic balance with their phosphorylation levels and maintaining overall protein content within a comparable range. Treatment with either LCP or DEX reduced the levels of these activated proteins, indicating a mitigation of the HAPE-induced overactivation of the PI3K/Akt pathway and the consequent exacerbation of pulmonary oxidative stress. It is noteworthy that p-PI3K expression returned to a level similar to that in the NC group. Based on the NO concentration data (Fig. 5A), the relative iNOS protein level in the LCP-M group was 0.41-fold that of the MOD group, suggesting that LCP prevented the excessive release of high-concentration NO triggered by oxidative stress *via* iNOS. Conversely, the relative eNOS protein level in the LCP-H group was 2.29-fold that of the NC group, promoting the gradual release of low-concentration NO. Through this dual modulation, LCP maintained NO within an appropriate and controllable range, thereby supporting vasodilation and suppressing oxidative stress responses.

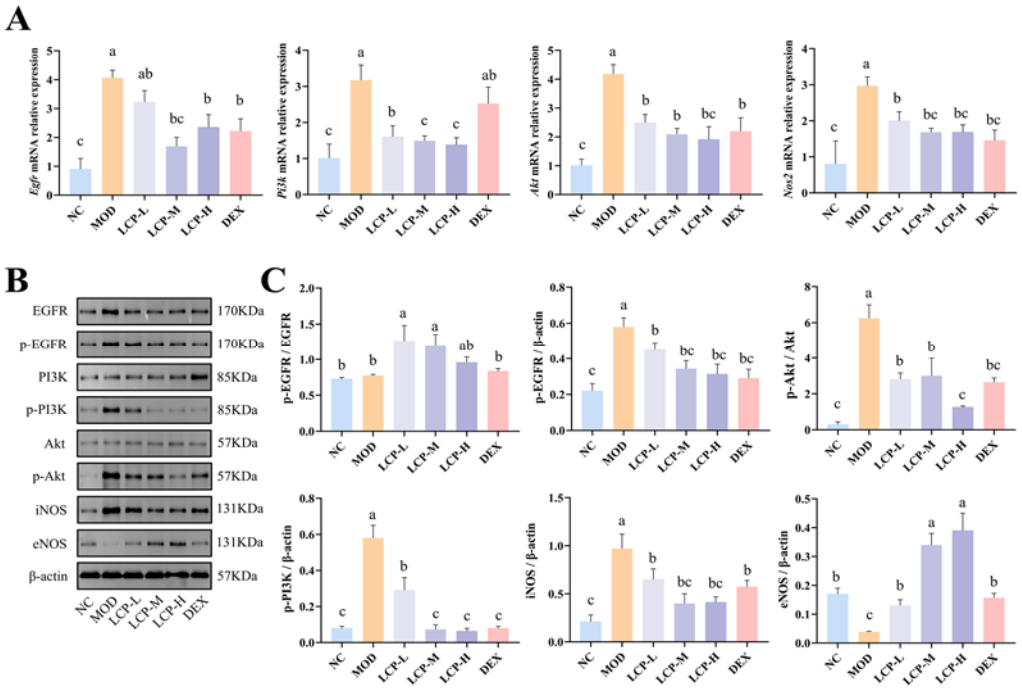


Fig. 6. Measurement of mRNA and protein levels of lung-related genes in mice. (A) Relative mRNA expression levels of *Egfr*, *Pi3k*, *Akt*, and *Nos2*. (B) Protein expression levels of EGFR, p-EGFR, PI3K, p-PI3K, Akt, p-Akt, iNOS, and eNOS determined by Western blot. (C) Quantitative analysis of protein expression. Experiments were performed in triplicate ($n = 3$). Different lowercase letters indicate statistically significant differences among groups ($P < 0.05$), while the same letter indicates no significant difference.

4. Discussion

HAPE is a critical and often fatal manifestation of acute mountain sickness (AMS)[33], characterized by rapid onset and severe clinical progression. Existing evidence indicates that its pathogenesis largely stems from increased pulmonary artery pressure along with the gradual buildup of inflammatory responses in the lungs under high-altitude hypobaric hypoxia. Previous studies indicate that certain natural products, including Potentilla anserina polysaccharides[30], Notoginsenoside R1[34] and *Lonicera caerulea* polyphenols, can effectively alleviate pulmonary edema by reducing oxidative stress and suppressing inflammation. Compared with synthetic therapeutic agents such as DEX[11] and nifedipine[13], LCP not only exhibit antioxidant activity but also offer distinct advantages, including low side effects, cost-effectiveness, and high safety, making them particularly attractive in HAPE therapeutic research. Utilizing such natural products to modulate vascular permeability, promote vasodilation, and inhibit pulmonary inflammation represents a promising therapeutic approach for HAPE[35].

Honeysuckle is an emerging cold-region berry rich in polyphenols, with anthocyanins constituting 36%-51% of its total polyphenol content, making them the most abundant polyphenols. This composition confers superior antioxidant, anti-inflammatory, and anti-hypoxic activities compared to many other natural products [36][37]. To date, the application of LCP in the prevention and treatment of HAPE remains unreported. Therefore, the present study was designed to explore the protective mechanisms of LCP against HAPE, with a focus on its anti-inflammatory effect.

We initially demonstrated that both LCP and SAL enhanced the hypoxic tolerance of PMVECs, with optimal effects observed at concentrations of 25, 15 μg·mL^{-1}, respectively. These treatments significantly mitigated intracellular oxidative stress injury. Apoptosis and cell cycle analyses demonstrated that hypoxia triggered S-phase arrest, likely through DNA replication stress or damage, leading to a shift from early apoptosis to late apoptosis or necrosis[38]. Consistent with previous reports[14], excessive ROS accumulation triggers both cell cycle arrest and apoptosis. By maintaining intracellular ROS at lower levels, LCP helped preserve normal cellular function and viability.

Following the establishment of the HAPE mouse model and oral administration of LCP, treatment with LCP at 400, 800, and 1200 mg·kg^{-1} was observed to confer several benefits. These included significant amelioration of body weight fluctuation and food intake, extension of survival time under normobaric hypoxia, and an increased survival rate in acute hypobaric hypoxia tests, albeit the absolute increases were moderate in scale. During the administration period, no notable variations were detected in terms of food intake, body weight, or daily behavior, and no toxic reactions were detected. In the network pharmacology screening stage, the bioavailability of the selected compounds met the effective threshold. These findings suggest that LCP may enhance the acclimatization of mice to high altitude conditions. Furthermore, LCP markedly reduced LWC, BALF, and the lung OI. Histopathological examination revealed that LCP alleviated thickening of the pulmonary vascular walls and accumulation of exudate in the alveolar spaces. These outcomes correspond to the enhanced performance in HAPE reported for other natural products such as notoginsenoside R1 and Potentilla anserina polysaccharide[30][34]. Compared to these individual substances like Quercetin and Luteolin in LCP, LCP has better efficacy, more comprehensive biological effects, and lower biotoxicity.

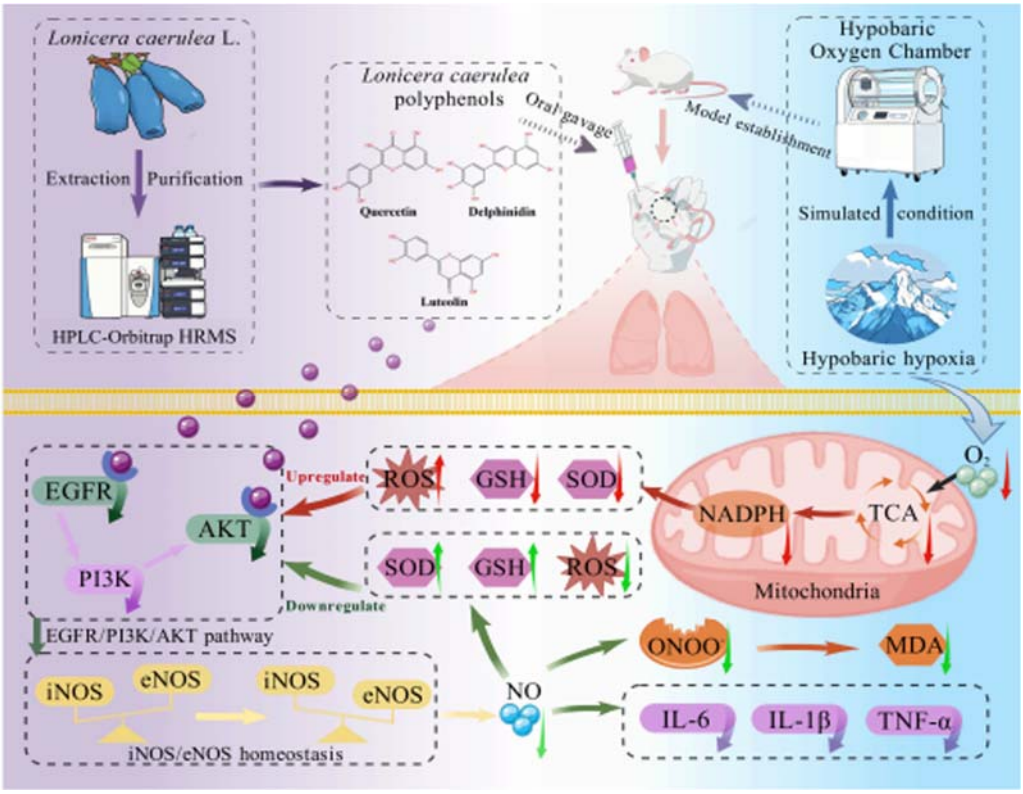


Fig. 7. Proposed action mechanism of LCP in the prevention and treatment of High-altitude pulmonary edema (HAPE).

Several studies have identified CAT, GSH, SOD, MDA, and NO as common biomarkers of oxidative stress injury, with their activities and concentrations varying according to the severity and duration of the insult[39][40]. Our assays revealed a sharp decline in the levels of CAT, SOD, and GSH following hypoxic exposure. Consistent with the literature, ROS and NO progressively accumulate under hypoxia. These species can directly oxidize the active sites of CAT and SOD, accelerate the degradation of these enzymes, and lead to a rapid loss of their activity[41]. Concurrently, GSH is increasingly consumed to counteract oxidative damage, while ROS-activated lipid peroxidation generates MDA and depletes NADPH, thereby inhibiting GSH regeneration[15]. Treatment with LCP significantly reduced NO concentration and restored the levels of these biomarkers to near normal ranges, reflecting its potent antioxidant capacity and its efficacy in mitigating the oxidative damage induced by HAPE (Fig. 7).

Measuring pro inflammatory cytokine levels in serum offers a valuable means to evaluate the severity of oxidative stress injury. IFN-γ and MCP-1 play crucial roles in the immune system, contributing to anti-tumor and immunoregulatory functions. We observed a decrease in IFN-γ levels under simulated high-altitude conditions. A possible explanation for this observation is that the excessive accumulation of ROS induced by high-altitude conditions inhibits the activity of the upstream transcription factor STAT4, a finding consistent with previous reports. Under oxidative stress, NF-κB acts as a positive regulator in the expression of multiple pro inflammatory cytokines, including MCP-1, TNF-α, IL-6, and IL-1β, thereby exacerbating oxidative damage and disrupting internal homeostasis[15][42][43][44]. Administration of LCP led to a marked reduction in the secretion of these pro inflammatory cytokines, which consequently reduced the load on the immune system.

LCP has excellent efficacy in preventing and treating HAPE, so we further studied its molecular mechanism. We initially characterized the components of purified LCP by LC Orbitrap HRMS, which led to the identification of 32 phenolic compounds, 20 flavonoids, and 12 phenolic acids along with other phenolics. Using network pharmacology, seven potentially bioactive compounds were subsequently screened. Molecular docking was then performed to further evaluate these candidates, resulting in the identification of 6 compounds (Quercetin, Pelargonidin, Luteolin, Isorhamnetin, Kaempferol, and Delphinidin) that showed binding energies $\leq$ -4.5 kcal·mol^{-1} against selected core targets. Among them, Quercetin, Luteolin, and Delphinidin demonstrated particularly robust binding to Akt and EGFR. Luteolin (a flavone) exhibited the strongest binding affinity to Akt, with a binding energy of -8.59 kcal·mol^{-1}. The GO and KEGG Enrichment analyses further predicted key regulatory genes and pathways, notably “positive regulation of nitric oxide biosynthetic process” and “nitrogen metabolism,” which are closely interconnected in nitrogen transformation, signaling molecule generation, and physiological regulation. This connection provides critical insights into the balance of nitrogen metabolism and the nitric oxide (NO) mediated regulatory network in vivo. It has been established that NO acts as a vasodilator and vascular remodeling agent, which can specifically alleviate pulmonary hypertension induced by HAPE and, at appropriate concentrations, exert anti-inflammatory effects[45]. In vivo, NO is primarily generated under the control of nNOS, iNOS, and eNOS

to maintain homeostasis[46]. iNOS is primarily regulated by the inflammatory status and can produce excessive NO, exacerbating inflammatory responses. Gradual expression of eNOS leads to a progressive increase in NO concentration, which at certain levels promotes vasodilation and alleviates HAPE symptoms[22][31]. nNOS is primarily localized in the nervous system[47], and does not participate in the regulation of pulmonary vascular tone during the pathogenesis of HAPE[48]. Both iNOS and eNOS are regulated by the PI3K/Akt pathway[22]错误!不能识别的开关参数。. In contexts such as cancer therapy and mitigation of oxidative stress, EGFR can modulate PI3K expression[49]. The integrated application of network pharmacology and molecular docking further pinpointed EGFR and Akt as pivotal targets, with Akt expression being closely linked to PI3K[39][50]. Luteolin and cyanidin are known to alleviate oxidative stress by acting on the EGFR/PI3K/Akt pathway[8],[51]. This supports the possibility that LCP mitigates HAPE symptoms by regulating iNOS and eNOS through the same pathway (Fig. 7).

EGFR is a prominent gene of interest in studies on cell proliferation and angiogenesis. The exploration of EGFR inhibitors has shown potential not only to delay cancer progression but also to exert positive effects on a variety of other pathological conditions[52][53]. Prior work has shown that targeting the EGFR/PI3K/Akt signaling axis can alleviate pathologies including inflammatory bowel disease and curb their advancement[54]. Based on our experimental results, EGFR was assessed by ELISA and Western blotting, while *Egfr* mRNA levels were determined using qRT-PCR. These analyses revealed that hypobaric hypoxia promotes both the production and activation of EGFR to p-EGFR. LCP treatment significantly inhibited this process, thereby attenuating the phosphorylation and activation of downstream PI3K and Akt. This observation aligns with results reported by Qiao[52]. Analysis of iNOS and eNOS protein expression, along with iNOS mRNA levels, indicated that LCP suppressed iNOS overexpression. Concurrently, moderate activation of Akt promoted physiological eNOS activity, thereby maintaining a balanced NO level (Fig. 7).

5. Conclusion

In summary, LCP treatment enhanced hypoxia tolerance, reduced oxidative stress and apoptosis in PMVECs, and markedly alleviated pulmonary edema, inflammation and vascular permeability in a mouse HAPE model. LCP balanced iNOS/eNOS expression and maintained NO homeostasis via regulating the EGFR/PI3K/Akt pathway, thus ameliorating HAPE pathogenesis. This study clarifies the protective effects and mechanisms of LCP against HAPE, providing new strategies for high-altitude-related disorders.

However, several limitations exist. This study was performed only in cellular and murine models, with no human clinical trials conducted. In addition, long-term safety and efficacy of LCP have not been evaluated. Further clinical and long-term safety studies are therefore warranted to validate its translational potential.

Acknowledgements

We thank the financial support from the National Key R&D Program of China (2022YFD1600500), Zhejiang province key research and development programs (2023C02006) and the Key Research and Development Project of Zhejiang Province (2023C02046).

Declaration of competing interest

The authors report no conflicts of interest, financial or personal, that could have impacted the research described in this paper.

References

[1] L. Guo, J. Qiao, M.S. Mikhailovich, et al., Comprehensive structural analysis of anthocyanins in blue honeysuckle (*Lonicera caerulea* L.), bilberry (*Vaccinium uliginosum* L.), cranberry (Vaccinium macrocarpon Ait.), and antioxidant capacity comparison. Food Chemistry: X, 23 (2024) 101734. https://doi.org/10.1016/j.fochx.2024.101734.

[2] M. Jia, J. Luo, Z. Zhao, et al., Co-analysis of network pharmacology and metabolomics: revealing the mechanism of using mixed strains to produce multi-stage fermentation products of fresh blue honeysuckle (*Lonicera caerulea* L.) to against hyperlipidemia. Food Chemistry: X, 29 (2025) 102852. https://doi.org/10.1016/j.fochx.2025.102852.

[3] S. Liu, F. Meng, R. Sun, et al., Wheat starch-*Lonicera caerulea* berry polyphenols complex regulates blood glucose and improves intestinal flora in type 2 diabetic mice. Carbohydrate Polymers, 351 (2025) 123061. https://doi.org/10.1016/j.carbpol.2024.123061.

[4] Q. Xiang, Z. Xia, H. Liu, et al., Isolation and characterization of a hepatoprotective polysaccharide from *Lonicera caerulea* L. var. edulis Turcz. ex Herd. fruit against APAP-induced acute liver injury mice. International Journal of Biological Macromolecules, 275 (2024) 133426. https://doi.org/10.1016/j.ijbiomac.2024.133426.

[5] P. Han, S. Chu, J. Shen, et al., Quercetin-derived microbial metabolite DOPAC potentiates CD8+ T cell anti-tumor immunity via NRF2-mediated mitophagy. Cell Metabolism, 37 (2025) 2438-2454. https://doi.org/10.1016/j.cmet.2025.09.010.

[6] L. Yang, P. Pi, M. Zhang, et al., Copper ionophore complex ES-Cu synergizes with quercetin to target FDX1, promote cuproptosis, and reverse lenvatinib resistance in hepatocellular carcinoma cells. Journal of Advanced Research, (2025), https://doi.org/10.1016/j.jare.2025.08.066.

[7] Z. He, X. Li, Z. Wang, et al., Protective effects of luteolin against amyloid beta-induced oxidative stress and mitochondrial impairments through peroxisome proliferator-activated receptor γ-dependent mechanism in Alzheimer's disease. Redox Biology, 66 (2023) 102848. https://doi.org/10.1016/j.redox.2023.102848.

[8] M. Gu, Z. Pang, Luteolin inhibits inflammation and M1 macrophage polarization in the treatment of Pseudomonas aeruginosa-induced acute pneumonia through suppressing EGFR/PI3K/AKT/NF-κB and EGFR/ERK/AP-1 signaling pathways. Phytomedicine, 141 (2025) 156663. https://doi.org/10.1016/j.phymed.2025.156663.

[9] E.R. Swenson, P. Bärtsch, High-altitude pulmonary edema. Comprehensive Physiology, 2 (2012) 2753-2773. https://doi.org/10.1002/j.2040-4603.2012.tb00459.x.

[10] Q. Zhou, D. Wang, Y. Liu, et al., Solnatide demonstrates profound therapeutic activity in a rat model of pulmonary edema induced by acute hypobaric hypoxia and exercise. CHEST, 151 (2017) 658-667. https://doi.org/10.1016/j.chest.2016.10.030.

[11] J. Burtscher, H. Gatterer, B.A. Beidleman, et al., Dexamethasone for prevention of AMS, HACE, and HAPE and for limiting impairment of performance after rapid ascent to high altitude: a narrative review. Military Medical Research, 12 (2025) 48. https://doi.org/10.1186/s40779-025-00634-y.

[12] G. Savioli, I.F. Ceresa, G. Gori, et al., Pathophysiology and therapy of high-altitude sickness: Practical approach in emergency and critical care. Journal of Clinical Medicine, 11 (2022) 3937. https://doi.org/10.3390/jcm11143937.

[13] D. Simancas-Racines, I. Arevalo-Rodriguez, D. Osorio, et al., Interventions for treating acute high altitude illness. Cochrane Database of Systematic Reviews, 6 (2018) CD009567. https://doi.org/10.1002/14651858.CD009567.pub2.

[14] M. Isaq, Y.L. Ramachandra, P.S. Rai, et al., Biogenic synthesized silver nanoparticles using fungal endophyte Cladosporium oxysporum of Vateria indica induce apoptosis in human colon cancer cell line via elevated intracellular ROS generation and cell cycle arrest. Journal of Molecular Liquids, 386 (2023) 122601. https://doi.org/10.1016/j.molliq.2023.122601.

[15] Q. Liu, X. Ding, X. Xu, et al., Tumor-targeted hyaluronic acid-based oxidative stress nanoamplifier with ROS generation and GSH depletion for antitumor therapy. International Journal of Biological Macromolecules, 207 (2022) 771-783. https://doi.org/10.1016/j.ijbiomac.2022.03.139.

[16] S. Sharma, Y. Singh, R. Sandhir, et al., Mitochondrial DNA mutations contribute to high altitude pulmonary edema via increased oxidative stress and metabolic reprogramming during hypobaric hypoxia. Biochimica et Biophysica Acta (BBA) - Bioenergetics, 1862 (2021) 148431. https://doi.org/10.1016/j.bbabio.2021.148431.

[17] C. Wang, H. Jiang, J. Duan, et al., Exploration of acute phase proteins and inflammatory cytokines in early stage diagnosis of acute mountain sickness. High Altitude Medicine & Biology, 19 (2018) 170-177. https://doi.org/10.1089/ham.2017.0126.

[18] Y. Hou, Y. Zhang, S. Jiang, et al., Salidroside intensifies mitochondrial function of CoCl2-damaged HT22 cells by stimulating PI3K-AKT-MAPK signaling pathway. Phytomedicine, 109 (2023) 154568. https://doi.org/10.1016/j.phymed.2022.154568.

[19] J. Lundeberg, J.R. Feiner, A. Schober, et al., Increased cytokines at high altitude: Lack of effect of ibuprofen on acute mountain sickness, physiological variables, or cytokine levels. High Altitude Medicine & Biology, 19 (2018) 249-258. https://doi.org/10.1089/ham.2017.0144.

[20] Z.J. McKenna, B.N. Bellovary, J.B. Ducharme, et al., Circulating markers of intestinal barrier injury and inflammation following exertion in hypobaric hypoxia. European Journal of Sport Science, 23 (2023) 2002-2010. https://doi.org/10.1080/17461391.2023.2203107.

[21] A. Ullah, R.K. Singla, Y. Zhang, et al., Understanding the mechanistic and therapeutic perspectives on cytokines and chemokines in acute high-altitude illness syndromes. Journal of Pharmaceutical Analysis, 15 (2025) 101249. https://doi.org/10.1016/j.jpha.2025.101249.

[22] C. Liu, M. Lin, J. Dai, et al., Ultrasound-activated directional and controllable nitric oxide therapy for vascular calcification repair through the modulation of eNOS/iNOS homeostasis. Acta Biomaterialia, 206 (2025) 297-311. https://doi.org/10.1016/j.actbio.2025.09.024.

[23] M. Maggiorini, Prevention and treatment of high-altitude pulmonary edema. Progress in Cardiovascular Diseases, 52 (2010) 500-506. https://doi.org/10.1016/j.pcad.2010.03.001.

[24] A. Chaovanalikit, M.M. Thompson, R.E. Wrolstad, Characterization and quantification of anthocyanins and polyphenolics in blue honeysuckle (*Lonicera caerulea* L.). Journal of Agricultural and Food Chemistry, 52 (2004) 848-852. https://doi.org/10.1021/jf030509o.

[25] N Zadeh, G Zeppa, Recovery and concentration of polyphenols from roasted hazelnut skin extract using macroporous resins. Foods, 11 (2022) 1969. https://doi.org/10.3390/foods11131969.

[26] N. Zhang, S. Tang, J. Zhang, et al., The dipeptidyl peptidase-4 inhibitor linagliptin ameliorates LPS-induced acute lung injury by maintenance of pulmonary microvascular barrier via activating the Epac1/AKT pathway. Biomedicine & Pharmacotherapy, 155 (2022) 113704. https://doi.org/10.1016/j.biopha.2022.113704.

[27] J. Jiang, H. Ouyang, Q. Zhou, et al., LPS induces pulmonary microvascular endothelial cell barrier dysfunction by upregulating ceramide production. Cellular Signalling, 92 (2022) 110250. https://doi.org/10.1016/j.cellsig.2022.110250.

[28] W. Jing, J. Cui, Y. Fu, et al., A novel method for multiple cytokines/chemokines DropArray assay in 5μL of bronchoalveolar lavage fluid (BALF) in mice. Sensors and Actuators B: Chemical, 242 (2017) 195-201. https://doi.org/10.1016/j.snb.2016.10.139.

[29] F. Luan, M. Li, K. Han, et al., Phenylethanoid glycosides of Phlomis younghusbandii Mukerjee ameliorate acute hypobaric hypoxia-induced brain impairment in rats. Molecular Immunology, 108 (2019) 81-88. https://doi.org/10.1016/j.molimm.2019.02.002.

[30] J. Shi, Z. Liu, M. Li, et al., Polysaccharide from *Potentilla anserina* L ameliorate pulmonary edema induced by hypobaric hypoxia in rats. Biomedicine & Pharmacotherapy, 139 (2021) 111669. https://doi.org/10.1016/j.biopha.2021.111669.

[31] B. Kusznierewicz, A. Piekarska, B. Mrugalska, et al., Phenolic composition and antioxidant properties of polish blue-berried honeysuckle genotypes by HPLC-DAD-MS, HPLC postcolumn derivatization with ABTS or FC, and TLC with DPPH visualization. Journal of Agricultural and Food Chemistry, 60 (2012) 1755-1763. https://doi.org/10.1021/jf2039839.

[32] M.A. Farag, M.H. Baky, I. Morgan, et al., Comparison of Balanites aegyptiaca parts: metabolome providing insights into plant health benefits and valorization purposes as analyzed using multiplex GC-MS, LC-MS, NMR-based metabolomics, and molecular networking. RSC Advances, 13 (2023) 21471-21493. https://doi.org/10.1039/D3RA03141A.

[33] H. Fruehauf, S.R. Vavricka, T.A. Lutz, et al., Evaluation of acute mountain sickness by unsedated transnasal esophagogastroduodenoscopy at high altitude. Clinical Gastroenterology and Hepatology, 18 (2020) 2218-2225.e2. https://doi.org/10.1016/j.cgh.2019.11.036.

[34] D. Huang, Y. Wang, C. Pei, et al., Pre-treatment with notoginsenoside R1 from Panax notoginseng protects against high-altitude-induced pulmonary edema by inhibiting pyroptosis through the NLRP3/caspase-1/GSDMD pathway. Biomedicine & Pharmacotherapy, 180 (2024) 117512. https://doi.org/10.1016/j.biopha.2024.117512.

[35] K.J. Dunham-Snary, D. Wu, E.A. Sykes, et al., Hypoxic Pulmonary Vasoconstriction: From Molecular Mechanisms to Medicine. Chest, 151 (2017) 181-192. https://doi.org/10.1016/j.chest.2016.09.001.

[36] R. Becker, A. Szakiel, Phytochemical characteristics and potential therapeutic properties of blue honeysuckle *Lonicera caerulea* L. (Caprifoliaceae). Journal of Herbal Medicine, 16 (2019) 100237. https://doi.org/10.1016/j.hermed.2018.10.002.

[37] M. Zhang, X. Ma, Z. Xiao, et al., Polyphenols in twenty cultivars of blue honeysuckle (*Lonicera caerulea* L.): Profiling, antioxidant capacity, and α-amylase inhibitory activity. Food Chemistry, 421 (2023) 136148. https://doi.org/10.1016/j.foodchem.2023.136148.

[38] J. Chen, F. Li, J. Yang, et al., Carbon dots and DNA: DNA binding mechanisms and their effect on the cell cycle arrest. Journal of Advanced Research, 2025, https://doi.org/10.1016/j.jare.2025.11.004.

[39] J.J. Batista, F.C.O. Silva, M.I.F. Araújo, et al., Parkia pendula polysaccharides have no acute toxicity and prevent ethanol-induced gastric ulcers via downregulation of TBARS, IL-6, and TNF-α and upregulation of SOD, CAT, and IL-10. International Journal of Biological Macromolecules, 309 (2025) 142702. https://doi.org/10.1016/j.ijbiomac.2025.142702.

[40] P. Sa-nguanpong, P. Wetprasit, U. Chatturong, et al., Protective effects of Sacha inchi meal protein hydrolysate against oxidative stress and endothelial dysfunction via MDA suppression and SOD activation in L-NAME-induced hypertensive rats. European Journal of Medicinal Chemistry Reports, 15 (2025) 100297. https://doi.org/10.1016/j.ejmcr.2025.100297.

[41] L.B. Menezes, B.B. Segat, H. Tolentino, et al., ROS scavenging of SOD/CAT mimics probed by EPR and reduction of lipid peroxidation in S. cerevisiae and mouse liver, under severe hydroxyl radical stress condition. Journal of Inorganic Biochemistry, 239 (2023) 112062. https://doi.org/10.1016/j.jinorgbio.2022.112062.

[42] Y. Geng, J. Yang, X. Cheng, et al., A bioactive gypenoside (GP-14) alleviates neuroinflammation and blood brain barrier (BBB) disruption by inhibiting the NF-κB signaling pathway in a mouse high-altitude cerebral edema (HACE) model. International Immunopharmacology, 108 (2022) 108675. https://doi.org/10.1016/j.intimp.2022.108675.

[43] J. Liu, P. Yu, X. Lai, et al., Siwei Jianghuang Decoction mitigates diabetic nephropathy by suppressing oxidative stress, inflammation and apoptosis via the inhibition of the NOX-4/NF-κB/MCP-1 pathway. Journal of Ethnopharmacology, 353 (2025) 120290. https://doi.org/10.1016/j.jep.2025.120290.

[44] M. Si, Y. Hu, Z. Jin, et al., NF-κB and pulmonary hypertension: Advances in mechanistic research and therapeutic applications. American Heart Journal Plus: Cardiology Research and Practice, 60 (2025) 100669. https://doi.org/10.1016/j.ahjo.2025.100669.

[45] J. Park, S. Shin, Y. Kim, et al., Vasorelaxant and antihypertensive effects of the Cibotii Rhizoma hydroethanolic extract via the PI3K/AKT/eNOS Pathway. Phytomedicine, 148 (2025) 157437. https://doi.org/10.1016/j.phymed.2025.157437.

[46] Z. Lacza, J.A. Snipes, J. Zhang, et al., Mitochondrial nitric oxide synthase is not eNOS, nNOS or iNOS. Free Radical Biology and Medicine, 35 (2003) 1217-1228. https://doi.org/10.1016/S0891-5849(03)00510-0.

[47] A. Anwar, D. Yameen, M. Masood, et al., Neuronal Nitric Oxide Synthase (nNOS) uncoupling in ischemic stroke: Mechanisms of oxidative/nitrosative stress and opportunities for neuroprotection: A review. International Journal of Biological Macromolecules, 332 (2025) 148589. https://doi.org/10.1016/j.ijbiomac.2025.148589.

[48] K.A. Fagan, R.C. Tyler, K. Sato, et al., Relative contributions of endothelial, inducible, and neuronal NOS to tone in the murine pulmonary circulation. American Journal of Physiology-Lung Cellular and Molecular Physiology, 277 (1999) 472-478. https://doi.org/10.1152/ajplung.1999.277.3.L472.

[49] T. Jin, L. Wang, R. Zhang, et al., Brain abundant membrane attached signal protein 1 regulates macrophage polarization through EGFR/PI3K/AKT signaling in renal cell carcinoma. International Journal of Biological Macromolecules, 330 (2025) 148268. https://doi.org/10.1016/j.ijbiomac.2025.148268.

[50] A. Abulizi, J. Simayi, M. Nuermaimaiti, et al., Quince extract resists atherosclerosis in rats by down-regulating the EGFR/PI3K/Akt/GSK-3β pathway. Biomedicine & Pharmacotherapy, 160 (2023) 114330. https://doi.org/10.1016/j.biopha.2023.114330.

[51] S. Gao, T. Chen, M.Y. Choi, et al., Cyanidin reverses cisplatin-induced apoptosis in HK-2 proximal tubular cells through inhibition of ROS-mediated DNA damage and modulation of the ERK and AKT pathways. Cancer Letters, 333 (2013) 36-46. https://doi.org/10.1016/j.canlet.2012.12.029.

[52] K. Qiao, Z. Yang, Y. Fang, et al., Salvigenin inhibits gastric cancer progression by suppressing the EGFR/PI3K/AKT pathway. Biochemical and Biophysical Research Communications, 784 (2025) 152645. https://doi.org/10.1016/j.bbrc.2025.152645.

[53] X. Wang, C. Wang, Y. Ma, et al., Discovery of a novel EGFR PROTAC degrader against C797S resistance mutation with potent antitumor efficacy in NSCLC treatment. Journal of Medicinal Chemistry, 68 (2025) 14569-14593. https://doi.org/10.1021/acs.jmedchem.5c00693.

[54] B.X. Mu, Y. Li, N. Ye, et al., Understanding apoptotic induction by *Sargentodoxa cuneata-Patrinia villosa* herb pair via PI3K/AKT/mTOR signalling in colorectal cancer cells using network pharmacology and cellular studies. Journal of Ethnopharmacology, 319 (2024) 117342. https://doi.org/10.1016/j.jep.2023.117342.